C. R. Mecanique 343 (2015) 219–231

Contents lists available at ScienceDirect

Comptes Rendus Mecanique

www.sciencedirect.com

A 0-D flame wrinkling equation to describe the turbulent flame surface evolution in SI engines

Stéphane Richard [a,*], Denis Veynante [b]

[a] IFP Énergies nouvelles, 1–4, avenue du Bois-Préau, 92852 Rueil-Malmaison cedex, France
[b] Laboratoire EM2C, CNRS École centrale Paris, Grande Voie des Vignes, 92295 Châtenay-Malabry cedex, France

ARTICLE INFO

Article history:
Received 22 March 2014
Accepted 4 September 2014
Available online 17 November 2014

Keywords:
0-D engine simulation
3-D model reduction
Spark-ignition
Flame kernel growth
Coherent Flame Model

ABSTRACT

The current development of reciprocating engines relies increasingly on system simulation for both design activities and conception of algorithms for engine control. These numerical simulation tools require high computational efficiencies, as calculations have to be performed in times close to real-time. Then, they are today mainly based on simple empirical laws to describe the combustion processes in the cylinders. However, with the rapid evolution of emission regulations and fuel formulation, more and more physics is expected in combustion models. A solution consists in reducing 3-D combustion models to build 0-dimensional models that are both CPU-efficient and based on physical quantities. This approach has been used in a previous work to reduce the 3-D ECFM (Extended Coherent Flame Model), leading to the so-called CFM1D. A key feature of the latter is to be based on a 0-D equation for the flame wrinkling derived from the 3-D equation for the flame surface density. The objective of this paper is to present in details the theoretical derivation of the wrinkling equation and the underlying modeling assumptions as well. Academic validations are performed against experimental data for several turbulence intensities and fuels. Finally, the proposed model is applied to engine simulations for a wide range of operating conditions. Comparisons are successfully conducted between in-cylinder measurements and the model predictions, highlighting the interest of reducing 3-D CFD models for calculations performed in the context of system simulation.

1. Introduction

System simulation is today increasingly exploited in the design process of internal combustion engines. Few years ago, its use was restricted to the evaluation of air-path configurations, but it has been recently extended to the development of engine control strategies thanks to the new real-time capabilities of 0-D engine simulators [1–3], which can now partially replace engine benches. In a near future, system simulation could also be used more intensively in the design process of combustion systems to recommend optimal engine settings (ignition and injection timings, fuel, air–ratios...), geometrical dimensions (compression ratio, bore and stroke...), or to evaluate the effect of new fuels on the engine behavior, as illustrated in recent works [4,5]. In the past, models used to compute the in-cylinder heat release were mainly based on simple 0-dimensional empirical laws [6,7] characterized by a high CPU efficiency. However, considering the stringency of pollutants and greenhouse gas emission standards, these approaches today suffer from a lack of predictivity to correctly describe all

* Corresponding author. Present address: Turbomeca, 64511 Bordes Cedex, France.
E-mail address: stephane.richard@graduates.centraliens.net (S. Richard).

http://dx.doi.org/10.1016/j.crme.2014.09.003
1631-0721/

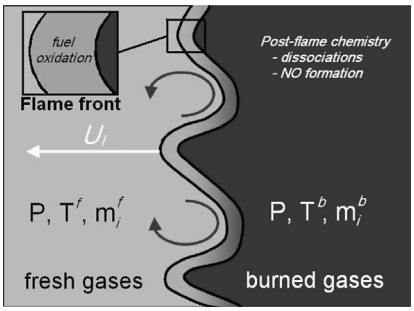

Fig. 1. The coherent flame approach (subscripts f and b respectively refer to fresh and burned gases).

the processes occurring in combustion chambers. To this purpose, 3-D CFD simulation tools could be coupled with 0-D or 1-D models for the air-path, but the required computational resources are still too important to make it an industrial tool for engineers in a near future. An interesting alternative to this coupling is to perform 3-D models reduction [8–10] in order to build 0-D models, whose behavior remains based on physical quantities while being very CPU-efficient. This approach has been used in a previous work [10] to derive the CFM1D model from the 3-D ECFM (Extended Coherent Flame Model), widely exploited in RANS [11] and LES [12] applications. A key point of CFM1D is that the flame wrinkling evolution is described by a new 0-D equation derived from the flame surface density (FSD) transport equation of ECFM. CFM1D was successfully applied to the combustion of gasoline [10], methane [13] or ethanol blends [14] in SI engines but no academic validation was conducted to check the intrinsic quality of the reduction methodology. The objective of this paper is thus to present in details the theoretical bases of the flame wrinkling equation as well as the underlying assumptions. Detailed validations are performed simulating an experiment relative to the ignition and flame propagation in an open vessel [15]. Finally, several operating conditions of a 4-cylinder engine are simulated and in-cylinder pressure and turbulent flame surface results are compared with experimental data.

2. The CFM1D combustion model

In a previous work, the CFM1D combustion model was proposed, based on several assumptions [10]:

- the mixture is an ideal gas;
- the domain in decomposed into two zones, fresh and burned gases, in which the mixture composition is assumed to be homogeneous;
- the pressure is identical in each zone;
- each zone is described by its mass, volume, composition and temperature;
- the turbulent kinetic energy is assumed to be uniform in the cylinder;
- fuel can be found either in a gas or liquid phase. This latter is then regarded as an isolated thermodynamic system exchanging mass and enthalpy with fresh gases.

In CFM1D, the heat released by combustion processes, $\mathrm{d}Q_{\mathrm{comb}}$, is expressed as:

$$\frac{\mathrm{d}Q_{\mathrm{comb}}}{\mathrm{d}t} = \sum_i h_{\mathrm{f},i} \left(\left.\frac{\mathrm{d}m_i}{\mathrm{d}t}\right|_{\mathrm{ff}} + \left.\frac{\mathrm{d}m_i}{\mathrm{d}t}\right|_{\mathrm{pf}} \right) \tag{1}$$

where $h_{\mathrm{f},i}$ is the formation enthalpy of species i, $\mathrm{d}m_i|_{\mathrm{ff}}$ and $\mathrm{d}m_i|_{\mathrm{pf}}$ are the mass variations of this species, respectively in the flame front due to reactions of fuel oxidation and in the burned gases due to post-flame chemistry reactions (Fig. 1). Post-flame chemistry contains two contributions [16]: the first one corresponds to dissociation processes (typically, $\mathrm{CO} \leftrightarrow \mathrm{CO_2}$), which are computed considering a tabulated time scale required to reach the chemical equilibrium, while the second one concerns NO formation, which is described following a similar approach. The species consumption rate through the flame writes:

$$\left.\frac{\mathrm{d}m_i}{\mathrm{d}t}\right|_{\mathrm{ff}} = -\nu_i \frac{W_i}{W_{\mathrm{fuel}}} \rho^{\mathrm{f}} Y^{\mathrm{f}}_{\mathrm{fuel}} U_{\mathrm{l}} S_{\mathrm{tot}} \tag{2}$$

where ρ^{f} is the fresh gases density, $Y^{\mathrm{f}}_{\mathrm{fuel}}$ is the fuel mass fraction in the fresh gases and U_{l} is the laminar flame speed estimated from a correlation depending on the nature of the fuel [10,14,17]. W_i denotes the molecular weight of the species i and ν_i is the stoichiometric coefficient corresponding to the reaction of fuel oxidation. Finally, S_{tot} is the total flame surface, which is estimated in the following section.

3. The 0-dimensional flame wrinkling equation

3.1. The unclosed 0-dimensional flame wrinkling equation

The model for the total flame surface basically comes from the transport equation of the filtered flame surface density $\overline{\Sigma}$, measuring the flame surface per unit volume [18]:

$$\begin{aligned}\frac{\partial \overline{\Sigma}}{\partial t} + \nabla \cdot \left(\langle \mathbf{u} \rangle_s \overline{\Sigma}\right) &= \langle \nabla \cdot \mathbf{u} - \mathbf{nn} : \nabla \mathbf{u} \rangle_s \overline{\Sigma} \\ &\quad - \nabla \cdot \left(\langle U_\mathrm{d} \mathbf{n} \rangle_s \overline{\Sigma}\right) \\ &\quad + \langle U_\mathrm{d} \nabla \cdot \mathbf{n} \rangle_s \overline{\Sigma}\end{aligned} \tag{3}$$

where $\mathbf{n} = -\nabla c/|\nabla c|$ is the local normal vector to the flame front pointing towards the fresh gases and $< \phi >_s = \overline{\phi \Sigma}/\overline{\Sigma}$ is the conditioned averaged value of ϕ along the flame surface, $\mathbf{u}$ is the local speed of the gases and U_d is the displacement speed of an iso-surface of the progress variable c.

A flame wrinkling factor Ξ can be defined as:

$$\Xi = \frac{\overline{\Sigma}}{|\nabla \bar{c}|} \tag{4}$$

where $\bar{.}$ stands for the spatial filter.

Weller et al. [19] proposed a transport equation for the flame wrinkling, but the latter can not be integrated for obtaining a 0-D model because the flame wrinkling is an intensive quantity. The approach adopted in this paper is nevertheless quite close.

A filter of characteristic length scale Δ, larger than the turbulence integral length scale l_t, is introduced, leading to consider all the flame wrinkling at the non-resolved scale level. Assuming a homogeneous and isotropic turbulence (HIT), the wrinkling is homogeneously distributed along the flame front, which gives:

$$\int_\Omega \overline{\Sigma} \delta V = \int_\Omega \Xi |\nabla \bar{c}| \delta V = \Xi \int_\Omega |\nabla \bar{c}| \delta V \tag{5}$$

yet $\int_\Omega \overline{\Sigma} \delta V = S_\mathrm{tot}$ and $\int_\Omega |\nabla \bar{c}| \delta V = S_\mathrm{res}$, where S_res is the resolved flame surface and Ω is the integration domain (*i.e.* the combustion chamber for an engine). Then:

$$S_\mathrm{tot} = \Xi S_\mathrm{res} \tag{6}$$

Hence:

$$\frac{1}{\Xi}\frac{\mathrm{d}\Xi}{\mathrm{d}t} = -\frac{1}{S_\mathrm{res}}\frac{\mathrm{d}S_\mathrm{res}}{\mathrm{d}t} + \frac{1}{S_\mathrm{tot}}\frac{\mathrm{d}S_\mathrm{tot}}{\mathrm{d}t} \tag{7}$$

Both terms on the right-hand side of Eq. (7) have now to be closed. The first one corresponds to the resolved flame strain and is identified in the following as κ_res, while the second one, κ_tot, represents the total flame strain.

3.2. κ_res term evaluation

The 0-dimensional consumption rate of a flame of surface S_tot results from the integration of the burned mass fraction transport equation:

$$\frac{\mathrm{d}m^\mathrm{b}}{\mathrm{d}t} = \rho^\mathrm{f} U_\mathrm{l} S_\mathrm{tot} = \rho^\mathrm{f} U_\mathrm{l} \Xi S_\mathrm{res} \tag{8}$$

where m^b is the burned gases mass, U_l is the laminar flame speed and ρ^f is the density of the fresh gases. This consumption rate can also write:

$$\frac{\mathrm{d}m^\mathrm{b}}{\mathrm{d}t} = \frac{\mathrm{d}\rho^\mathrm{b} V^\mathrm{b}}{\mathrm{d}t} = \rho^\mathrm{b}\frac{\mathrm{d}V^\mathrm{b}}{\mathrm{d}t} + V^\mathrm{b}\frac{\mathrm{d}\rho^\mathrm{b}}{\mathrm{d}t} \tag{9}$$

where V^b and ρ^b are the burned gases volume and density respectively.

Considering a spark ignition engine configuration, as all the flame wrinkling is contained at the non-resolved scale level, the resolved flame front can be assumed spherical (Fig. 2). A burned gas radius r^b can then be defined as $V^\mathrm{b} = 4\pi {r^\mathrm{b}}^3/3$. Thus $S_\mathrm{res} = 4\pi {r^\mathrm{b}}^2$ and:

$$\frac{\mathrm{d}S_\mathrm{res}}{\mathrm{d}t} = \frac{2}{r^b}\frac{\mathrm{d}V^b}{\mathrm{d}t} \tag{10}$$

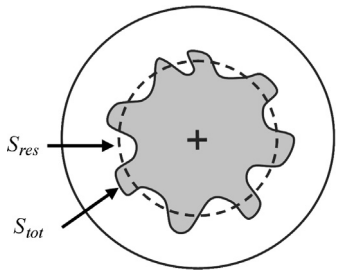

Fig. 2. Definition of the mean and total flame surfaces.

Combining all these relations with Eqs. (8) and (9) gives:

$$\frac{1}{S_{\text{res}}}\frac{\mathrm{d}S_{\text{res}}}{\mathrm{d}t} = \frac{2}{r^{\text{b}}}(1+\tau)\Xi U_{\text{l}} - \frac{2}{3}\frac{1}{\rho^{\text{b}}}\frac{\mathrm{d}\rho^{\text{b}}}{\mathrm{d}t} \tag{11}$$

where $1+\tau = \rho^{\text{f}}/\rho^{\text{b}}$ is the thermal expansion rate. The second term on the right-hand side integrates the compressibility effects and has to be estimated. Under the basic hypothesis of the CFM1D model (see Section 2), *i.e.* the burned gases are considered as perfect ones, the pressure is homogeneous in the combustion chamber ($P = P^{\text{b}}$, where P is the pressure and P^{b} is the burned gases' pressure), the burned gases' composition is constant and the evolution of these gases is isentropic during their dilation; it comes:

$$\frac{1}{\rho^{\text{b}}}\frac{\mathrm{d}\rho^{\text{b}}}{\mathrm{d}t} = \frac{1}{P}\frac{\mathrm{d}P}{\mathrm{d}t} - \frac{1}{P^{\frac{\gamma}{\gamma-1}}}\frac{\mathrm{d}P^{\frac{\gamma-1}{\gamma}}}{\mathrm{d}t} = \frac{1}{\gamma P}\frac{\mathrm{d}P}{\mathrm{d}t} \tag{12}$$

and Eq. (11) becomes:

$$\frac{1}{S_{\text{res}}}\frac{\mathrm{d}S_{\text{res}}}{\mathrm{d}t} = \frac{2}{r^{\text{b}}}(1+\tau)\Xi U_{\text{l}} - \frac{2}{3\gamma P}\frac{\mathrm{d}P}{\mathrm{d}t} \tag{13}$$

3.3. κ_{tot} term evaluation

The growth rate of the total flame surface can write:

$$\frac{\mathrm{d}S_{\text{tot}}}{\mathrm{d}t} = \frac{\mathrm{d}}{\mathrm{d}t}\int_{\Omega}\delta S = \frac{\mathrm{d}}{\mathrm{d}t}\int_{\Omega}\frac{\delta S}{\delta V}\delta V = \int_{\Omega}\frac{\mathrm{d}\overline{\Sigma}}{\mathrm{d}t}\delta V \tag{14}$$

Starting from Eq. (4) and regrouping the unsteady, convection and propagation terms to obtain a material derivative, leads to:

$$\frac{\mathrm{d}\overline{\Sigma}}{\mathrm{d}t} = \langle \nabla\cdot\mathbf{u} - \mathbf{nn}:\nabla\mathbf{u}\rangle_s\overline{\Sigma} + \langle U_{\text{d}}\nabla\cdot\mathbf{n}\rangle_s\overline{\Sigma} \tag{15}$$

Using Eq. (15) to express the flame surface density derivative in Eq. (14) and decomposing each contribution as the sum of a resolved and a non-resolved part, as made by Richard et al. [12], the following equation is obtained:

$$\frac{\mathrm{d}S_{\text{tot}}}{\mathrm{d}t} = \int_{\Omega}\big([S_{\text{res}} + S_{\text{sgs}}] + [C_{\text{res}} + C_{\text{sgs}}]\big)\delta V \tag{16}$$

where $S_{\text{res}} = (\nabla\cdot\tilde{\mathbf{u}} - \mathbf{NN}:\nabla\tilde{\mathbf{u}})\overline{\Sigma}$ represents the resolved strain rate acting on the flame due to the filtered flow field, $S_{\text{sgs}} = (\langle\nabla\cdot\mathbf{u} - \mathbf{nn}:\nabla\mathbf{u}\rangle_s - (\nabla\cdot\tilde{\mathbf{u}} - \mathbf{NN}:\nabla\tilde{\mathbf{u}}))\overline{\Sigma}$ is the non-resolved strain rate, $C_{\text{res}} = (U_{\text{d}}\nabla\cdot\mathbf{N})\overline{\Sigma}$ stands for the resolved curvature of the flame front and $C_{\text{sgs}} = (\langle U_{\text{d}}\nabla\cdot\mathbf{n}\rangle_s - U_{\text{d}}\nabla\cdot\mathbf{N})\overline{\Sigma}$ is the non-resolved curvature. Finally, $\mathbf{N} = -\nabla\tilde{c}/|\nabla\tilde{c}|$ is the normal to the resolved flame front.

Under the assumptions that the flame is globally spherical and infinitely thin, Eq. (16) can be rewritten in spherical coordinates (see Appendix A), which leads to the following expression:

$$\frac{1}{S_{\text{tot}}}\frac{\mathrm{d}S_{\text{tot}}}{\mathrm{d}t} = \frac{2}{r^{\text{b}}}(1+\tau)U_{\text{l}} + \frac{\int_{\Omega}[S_{\text{sgs}} + C_{\text{sgs}}]\delta V}{\int_{\Omega}\overline{\Sigma}\delta V} - \frac{2}{3\gamma P}\frac{\mathrm{d}P}{\mathrm{d}t} \tag{17}$$

A closure has now to be found for the second term occurring on the right-hand side of Eq. (17). To this purpose, the expressions proposed by Richard et al. [12] are retained, leading to:

$$\frac{\int_\Omega [S_{sgs}+C_{sgs}]\delta V}{\int_\Omega \overline{\Sigma}\delta V} = \frac{1}{\int_\Omega \overline{\Sigma}\delta V} \times \int_\Omega \left[\Gamma\left(\frac{u'}{U_l},\frac{l_t}{\delta_l}\right)\frac{u'}{l_t}\overline{\Sigma} + \beta_c U_l \frac{c^*-\bar{c}}{\bar{c}(1-\bar{c})}\left(\overline{\Sigma}-|\nabla\bar{c}|\right)\overline{\Sigma}\right]\delta V \tag{18}$$

where Γ is the efficiency function of Charlette et al. [20] (see Appendix B), u' is the velocity fluctuation, l_t the integral length scale, δ_l the laminar flame thickness (provided for example by the Blint correlation [21]), β_c and c^* are model constants.

Going further in the formal integration of Eq. (18) is hardly possible and closure has to be proposed at this stage. Thus, keeping in mind that the model is devoted to SI engine computations, a phenomenological closure close to the one of Weller et al. [19] is proposed. During the first instants following spark timing, the flame front is weakly wrinkled, *i.e.* $\overline{\Sigma} \approx |\nabla\bar{c}|$. The non-resolved curvature term is furthermore negligible compared to the non-resolved strain rate term. Then, assuming a homogeneous and isotropic turbulence (HIT), the strain rate is homogeneous along the flame front and Eq. (18) reduces to:

$$\frac{\int_\Omega S_{sgs}\delta V}{\int_\Omega \overline{\Sigma}\delta V} = \Gamma\left(\frac{u'}{U_l},\frac{l_t}{\delta_l}\right)\frac{u'}{l_t} \tag{19}$$

Curvature effects progressively balance the strain rate ones when flame wrinkling tends towards its equilibrium value. The latter can be supplied by a KPP analysis [12,22] (see Appendix C):

$$\Xi^{eq} = 1 + \frac{2}{U_l}\left(\frac{C\Gamma u'^2}{1-\beta_c c^*/(1+\tau)}\right)^{\frac{1}{2}} \tag{20}$$

where C is a model constant.

In order to take into account the evolution of the curvature effect during the progression of the flame wrinkling towards its equilibrium value, the strain rate term is corrected as follows:

$$\frac{\int_\Omega [S_{sgs}+C_{sgs}]\delta V}{\int_\Omega \overline{\Sigma}\delta V} = \Gamma\left(\frac{u'}{U_l},\frac{l_t}{\delta_l}\right)\frac{u'}{l_t}\left(\frac{\Xi^{eq}-\Xi}{\Xi^{eq}-1}\right) \tag{21}$$

Combining this equation with Eq. (19) leads to the following expression for the unresolved curvature:

$$\frac{\int_\Omega C_{sgs}\delta V}{\int_\Omega \overline{\Sigma}\delta V} = -\Gamma\left(\frac{u'}{U_l},\frac{l_t}{\delta_l}\right)\frac{u'}{l_t}\frac{\Xi-1}{\Xi^{eq}-1} \tag{22}$$

and the modeling proposed by Colin et al. [23] or Charlette et al. [20] for LES is recovered.

Finally, when the flame kernel is sufficiently small, it is not strained with the same efficiency by all the eddies. The strain efficiency of each vortex class for a planar flame is integrated in the Γ function, but the latter does not account for the specific case of a small flame kernel. Then, a characteristic time τ_l for the flame growth is introduced and is defined as the time required by the flame kernel to reach a diameter ζ (over-adiabaticity effects occurring during spark timing are neglected):

$$\tau_l = \frac{\zeta}{2(1+\tau)U_l} \tag{23}$$

For an eddy of size λ that evolves in a turbulence characterized by the fluctuating speed u' and the length scale l_t, the turnover time writes: $\tau_\lambda = \lambda/u'_\lambda$. Assuming the eddy lies in the inertial range of the Kolmogorov cascade, $u'_\lambda = (\lambda/l_t)^{\frac{1}{3}}u'$ and:

$$\tau_\lambda = l_t^{\frac{1}{3}}\lambda^{\frac{2}{3}}u'^{-1} \tag{24}$$

For a given time t and a characteristic length scale ζ of the flame kernel, an eddy is able to wrinkle the flame front after a turnover time if: $\tau_\lambda \le \tau_l$. Moreover, for the following typical values encountered in engine applications: $u' \approx 10\ \mathrm{m\,s^{-1}}$, $l_t \approx 5\cdot 10^{-3}$ m, $\tau \approx 4$, $U_l \approx 1\ \mathrm{m\,s^{-1}}$, it comes:

$$\lambda \le (\kappa\zeta)^{\frac{3}{2}} \tag{25}$$

where

$$\kappa = \frac{u'}{2(1+\tau)U_l l_t^{1/3}} \approx 5\ \mathrm{m}^{-1/3} \tag{26}$$

The evolution of $\lambda_{max} = (\kappa\zeta)^{\frac{3}{2}}$ during flame development is plotted in Fig. 3 as a function of ζ. For the conditions considered here, it is noticeable that roughly, the eddies larger than the flame kernel length scale are not able to wrinkle

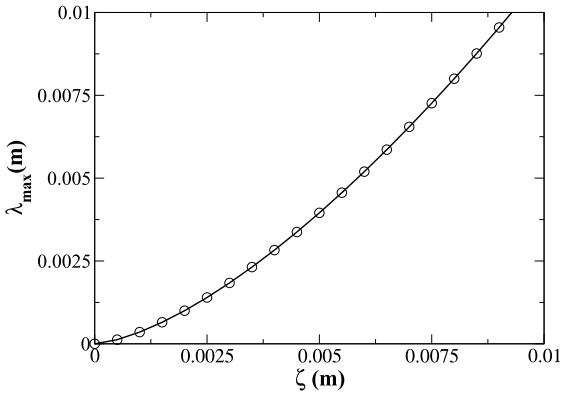

Fig. 3. Solution to the equation: $\lambda_{max} = (\kappa\zeta)^{\frac{3}{2}}$ ($\kappa = 5\ \mathrm{m}^{-\frac{1}{3}}$), where ζ and λ_{max} are length scales related respectively to the flame kernel and to the size of the largest eddy able to wrinkle the kernel surface.

the flame front. This trend stays true until the diameter reaches the integral length scale ($5 \cdot 10^{-3}$ m). This criterion is indicative, but provides an order of magnitude of the correction to incorporate into the strain rate term. The correction suggested by Mantel [24] or Richard et al. [12] is here retrieved. Thus, the strain rate is practically corrected considering only eddies for which the length scale is lower than the diameter of the flame kernel in the function Γ.

Eq. (17) finally writes:

$$\begin{aligned}\frac{1}{S_{tot}}\frac{\mathrm{d}S_{tot}}{\mathrm{d}t} = {} & \frac{2}{r^b}(1+\tau)U_l \\ & + \Gamma\left(\frac{u'_{\lambda_{max}}}{U_l}, \frac{\lambda_{max}}{\delta_l}\right)\frac{u'_{\lambda_{max}}}{\lambda_{max}}\left(\frac{\Xi^{eq}-\Xi}{\Xi^{eq}-1}\right) \\ & - \frac{2}{3\gamma P}\frac{\mathrm{d}P}{\mathrm{d}t}\end{aligned} \tag{27}$$

From Eqs. (7), (13) and (28) a 0-dimensional equation for the flame wrinkling evolution is deduced:

$$\frac{1}{\Xi}\frac{\mathrm{d}\Xi}{\mathrm{d}t} = \underbrace{\Gamma\left(\frac{u'_{\lambda_{max}}}{U_l}, \frac{\lambda_{max}}{\delta_l}\right)\frac{u'_{\lambda_{max}}}{\lambda_{max}}\left(\frac{\Xi^{eq}-\Xi}{\Xi^{eq}-1}\right)}_{Str_{turb}} \underbrace{- \frac{2}{r^b}(1+\tau)(\Xi-1)U_l}_{Str_{mean}} \tag{28}$$

where in practice λ_{max} is taken as: $\lambda_{max} = \min(2r^b, l_t)$.

Eq. (28) is similar to the equation of Weller et al. [19] for the local flame wrinkling and contains two terms in its right-hand side. The first one, Str_{turb}, corresponds to the strain of the flame front by the different eddies of the flow. As already mentioned, this strain rate does not account for the whole turbulence spectrum, but only the effects of the eddies able to wrinkle the flame front. For example, the eddies bigger than the flame kernel are too slow to affect the flame during its early growth.

The second term in the right-hand side of Eq. (28), Str_{mean}, stands for the impact of the mean strain rate due to thermal expansion and curvature. Indeed, the burned gases' dilatation tends to impose a positive curvature and to limit flame wrinkling. This phenomenon has already been highlighted in the DNS of Echekki et al. [25]. Such a term is also recovered in Weller's equation in the form of a resolved strain. It is also worth noticing the compressibility effects linked to the terms κ_{tot} and κ_{res} are balanced. This is probably due to the fact they have the same impact on the growth rates of a laminar surface and of a wrinkled surface.

It can be noticed that Eq. (28) can be rewritten as:

$$\frac{1}{\Xi}\frac{\mathrm{d}\Xi}{\mathrm{d}t} = A\frac{\Xi^{eq}-\Xi}{\Xi^{eq}-1} - B(\Xi-1) \tag{29}$$

where $A = \Gamma(\frac{u'_{\lambda_{max}}}{U_l}, \frac{\lambda_{max}}{\delta_l})\frac{u'_{\lambda_{max}}}{\lambda_{max}}$ and $B = \frac{2}{r^b}(1+\tau)U_l$. In this equation, Ξ tends towards Ξ^{eq} only if:

$$\Xi^{eq} = 1 \quad \text{or} \quad B \ll A \tag{30}$$

This last condition notably depends on the flame expansion speed $(1+\tau)U_l$.

The last point of the model concerns the computation of the resolved flame surface to obtain the total flame surface (Eq. (6)). Indeed, for the specific case of a spark ignition engine, the flame may interact with the combustion chamber walls, then modifying the available flame surface. For this purpose, S_{res} is tabulated *a priori* as a function of the piston position

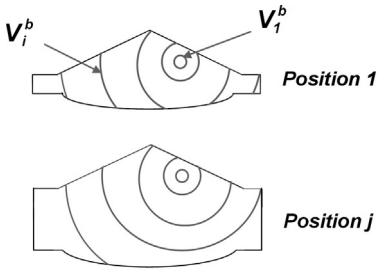

Fig. 4. Principle of the resolved flame surface tabulation.

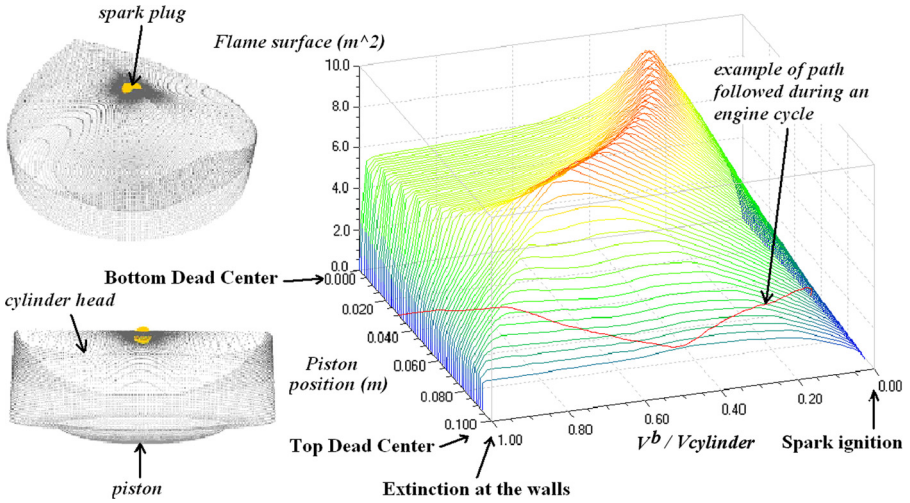

Fig. 5. (Color online.) Mean flame surface look-up table graphic representation.

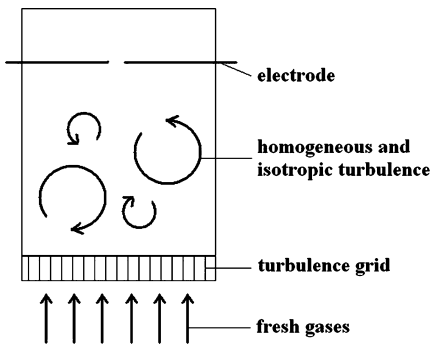

Fig. 6. Schematic representation of the experimental configuration of Renou et al. [15].

and burned gases volume (Fig. 4), assuming a spherical propagation of the resolved flame front from the spark plug towards the cylinder walls [10]. This tabulation takes into account the combustion chamber geometry and spark plug location and allows at each time step to retrieve the instantaneous resolved flame surface (Fig. 5).

4. Validation of the 0-D equation against experimental data in an open vessel

The experimental configuration of Renou et al. [15,26] was designed for studying spark-ignition cases in a turbulent and closed media (Fig. 6). A fresh gases mixture enters at a mean speed of 4 $\mathrm{m\,s^{-1}}$ in a square cross-section combustion chamber (width 80 mm) and is ignited by a pair of electrodes. Combustion then occurs in an HIT generated by a turbulence grid disposed upstream of the combustion chamber.

Several turbulence levels were reached depending on the grid choice: no turbulence, a first HIT parameterized by an integral length scale $l_t = 6$ mm and a fluctuating speed $u' = 0.18$ $\mathrm{m\,s^{-1}}$ and a second HIT for which $l_t = 6.5$ mm and

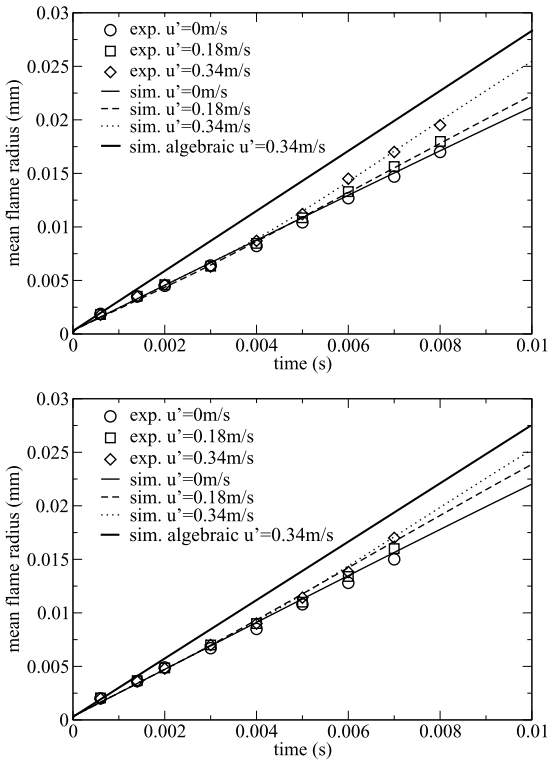

Fig. 7. Evolution of the resolved flame kernel radius r^b with time for different turbulence levels in the vessel. Top: propane. Bottom: methane. Bold lines correspond to the response of an algebraic model for Ξ.

$u' = 0.34\ \mathrm{m\,s^{-1}}$. These quantities were obtained by particle image velocimetry (PIV) and decreased weakly during the flame propagation time in the vessel.

The lengths of the flame contour were measured from high-speed laser tomography images. Two flame contours are of interest in the experiment: the mean and the turbulent contours. A mean radius r^b can be deduced along with a wrinkling factor comparable to Ξ. Measurements were performed for different fuels including methane and propane. Simulations were carried out for both fuels and all flow conditions using experimental values for u', l_t, U_l and δ_l in Eq. (28). The strain rate being not negligible during the early flame growth, the planar laminar flame speed $U_l{}^0$ provided by Renou et al. was here corrected using a Markstein length l determined from the experimental laminar flow cases:

$$U_l = U_l{}^0 - \frac{2l(1+\tau)U_l}{r^b} \tag{31}$$

Time evolutions of the mean radius r^b obtained from the simulations are shown in Fig. 7: the trends are satisfying for both fuels, the growth rate increasing with turbulence intensity. Moreover, the levels reached are in a good agreement with the experimental data, even if a slight overestimation is noticeable for methane, mainly in the laminar regime. It can be explained as follows: the corrections of the laminar flame speed, functions of the strain rate, may not be relevant for the high strain rates reached during early flame development.

Fig. 8 compares the flame wrinkling evolutions. In the laminar regime, flame wrinkling remains unity, then the corresponding results are not shown. For the turbulent cases, the predicted time evolutions of the flame wrinkling are very close to the experimental ones. Two points should be underlined: first of all, final flame wrinkling values are very well predicted, thanks to the Charlette efficiency function and experimental variations of the flame wrinkling are very well reproduced. The instants at which this wrinkling starts to grow is piloted by the length scale λ_{max}, while its slope is recovered thanks to the unsteady characteristic of Eq. (28). It should be noticed that such a behavior can not be reproduced by algebraic models for flame wrinkling often used in engine cycle simulations and which are based of an equilibrium assumption, *i.e.*: $\Xi(t) = \Xi^{equ}(t)$ (Figs. 7 and 8).

The relative contributions Str_{mean} and Str_{turb} of Eq. (28) are represented in Fig. 9: both are significant at the turbulence levels of the experiment, even if the effect of turbulent strain rates predominates. When the turbulent intensity increases, this latter contribution becomes more and more dominant until being preponderant at high turbulent intensities. In the cases studied here, the turbulent intensity remains quite weak ($0.5\ \mathrm{m\,s^{-1}} < u'/S_l < 1\ \mathrm{m\,s^{-1}}$) when compared to the levels encountered in engines ($1\ \mathrm{m\,s^{-1}} < u'/S_l < 10\ \mathrm{m\,s^{-1}}$) so that the turbulent strain may be even more predominant, which ensures the condition given by Eq. (30).

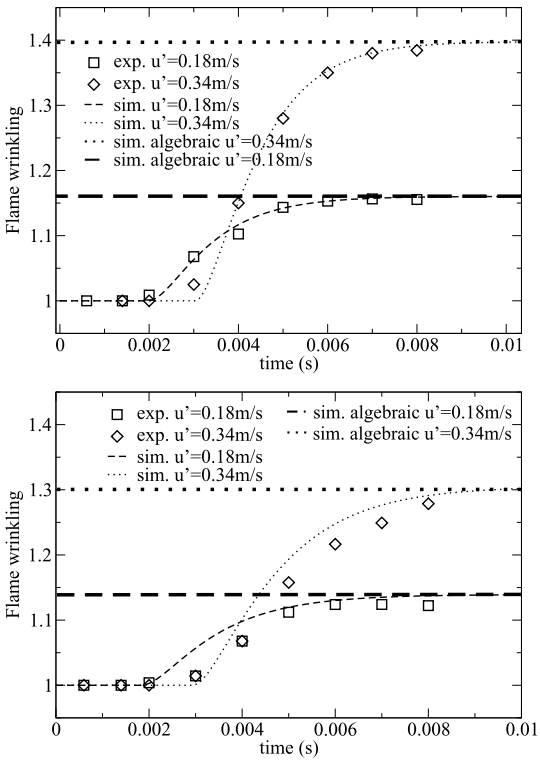

Fig. 8. Evolution of the flame wrinkling factor Ξ with time for different turbulence levels in the vessel. Top: propane. Bottom: methane. Bold lines correspond to the response of an algebraic model for Ξ.

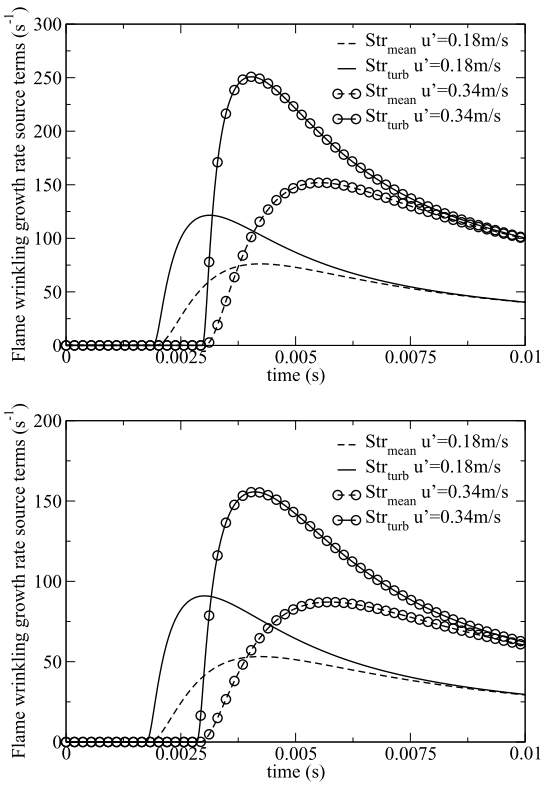

Fig. 9. Evolution of the flame wrinkling factor growth rate contributions Str_{mean} and Str_{turb} (Eq. (28)) with time for different turbulence levels in the vessel. Top: propane. Bottom: methane.

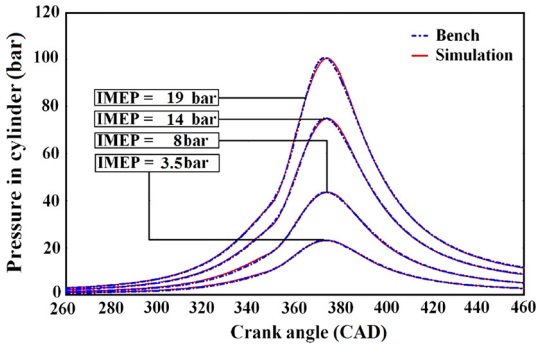

Fig. 10. Comparison between experimental and simulated in-cylinder pressure evolutions for various engine loads at 2500 rpm.

5. Application to a realistic engine configuration

The CFM1D has been implemented in a 1-D engine simulation software and tested on a single cylinder SI engine (displacement: 450 cm^3, compression ratio: 10.5) fueled with methane. An experimental database was available, comprising results at 2500 rpm for a wide range of loads from idle to Wide Open Throttle (Indicated Mean Effective Pressure (IMEP) from 3 to 20 bar). It should be noticed that for all operating conditions, a unity equivalence ratio was used on the engine.

5.1. Engine simulator set-up and calibration

The simulator is constituted by a number of components representing the different engine parts. The combustion model is embedded in the cylinder one and heat transfer at the walls are accounted with the classical Woschni model [27]. The boundary conditions (pressure and temperature) and engine settings (spark advance, injection timing and duration) are set from the experimental database.

Contrary to simple laboratory configurations, it is difficult to extract reliable information about turbulence properties—namely u' and l_t—from engine tests. However, such quantities are needed in order to solve the flame wrinkling equation (Eq. 28). Therefore, the 0-D turbulence model proposed in [10] is retained. Such a model solves equations for the mean K and turbulent k kinetic energies. Due to the complexity of SI engines geometries (air-path, combustion chamber, etc.) and of related flow fields, a calibration of the turbulence model is required for each new engine. The calibration methodology was presented in [10] and mainly aims at describing the effect of the geometry on the aerodynamics of the combustion chamber by setting the tumble number of the flow at intake valve closure (IVC) with the objective to correctly fit the maximum cylinder pressure. This tumble number can be seen as an initial condition of the simulation and is an image of the mean flow kinetic energy K at IVC. Then a 0-D equation for K is used to describe the progressive transfer of energy from the mean flow to the turbulent kinetic energy k through a source term in the 0-D equation for k. The turbulent velocity fluctuation u' is finally retrieved from k following: $u' = \sqrt{2/3k}$, while the integral length scale is described using a simple geometrical law [7]. Eq. (28) also requires the knowledge of the laminar flame thickness and velocity, which are here given by correlations proposed by Bougrine et al. [17] for methane.

5.2. Model validation against in-cylinder pressure measurements and combustion analysis

An example of simulated cylinder pressure curves for several engine loads is presented in Fig. 10. A very good agreement with experimental data is obtained for all operating conditions, demonstrating that the combination of the 0-D turbulence model proposed in [10] and the flame wrinkling equation well describes heat release by combustion.

A more detailed analysis can also be performed using advanced combustion analysis. Combustion analysis is a standard tool for the piston engines developers community and allows one to extract the energy released by flame propagation from the in-cylinder pressure trace by solving the first thermodynamic law. In the present paper, a classical two-zone combustion analysis is performed, giving also access to the evolution of the temperature, volume and composition of both fresh and burned gases. Combining Eqs. (1) and (2) and using the correlation of Bougrine et al. [17] for the laminar flame speed thus permits to obtain the total flame surface (S_{tot}) experimental variation in the engine cycle. This quantity is compared to the simulated ones in Fig. 11. Very small differences are highlighted for all engine conditions and remains mainly related to the initial flame kernel growth and flame interaction with the cylinder-liner phases. Such errors can be related either to the assumption of a perfectly spherical flame or to modeling hypotheses made to close the flame wrinkling equation. In the following, the latter statement is arbitrarily retained to compare experimental and numerical wrinkling factor evolutions, as presented in Fig. 12. The experimental trace is here obtained from the total flame surface using Eq. (6) assuming that the mean flame surface is the same as in the simulations. Such post-processing is a novelty and has the advantage to allow indirect measurements of flame wrinkling from classical combustion analysis. It can be concluded from Fig. 12 that the flame wrinkling equation proposed in this paper describes in a fair way the maximum wrinkling, but also its unsteady evolution from ignition to extinction at the walls.

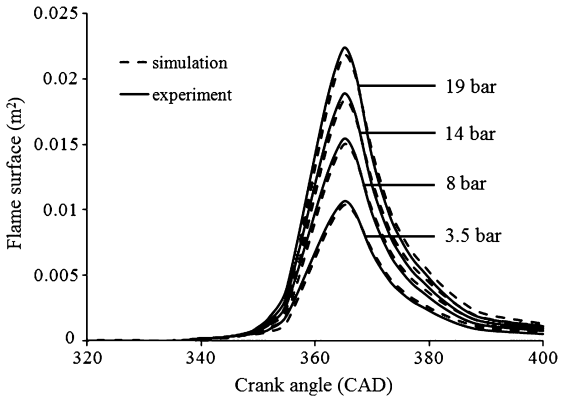

Fig. 11. Comparison between experimental and simulated flame surface evolutions for various engine loads at 2500 rpm.

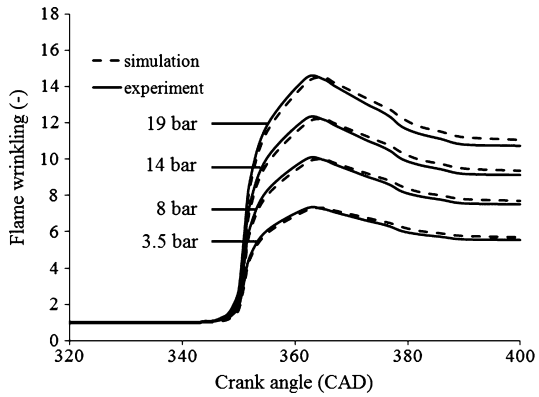

Fig. 12. Comparison between experimental and simulated flame wrinkling evolutions for various engine loads at 2500 rpm.

6. Conclusions

A reduction of the 3-D equation for the flame surface density was presented. This approach is close to the one adopted by Weller et al. in a 3-dimensional LES context, but was here conducted under the assumption of a spherical propagation of the flame starting from the spark-plug. Closures of the 0-D equation were validated against an experimental configuration for several turbulent intensities and fuels (propane and methane). The model was then successfully applied to engine simulations and allowed to well reproduce in-cylinder pressure measurements but also experimental evolutions of flame surface and wrinkling. To this end, a new methodology was proposed to extract such information from classical two-zone combustion analysis combining CFM1D equations with standard thermodynamic laws and conservation equations.

Finally, this kind of model is useful in the system simulation context for describing premixed combustion processes in SI engines [10,14,13]. However, it can also be used in 3-D simulations during the instants following sparking to describe the early flame kernel growth. In this case, the burned gases quantity indeed remains too small to ensure a proper flame propagation [19,28,29] and the combustion occurs mainly at the sub-grid scale thus needing for a sgs description of the wrinkling factor and the total flame surface.

Appendix A

Using spherical coordinates, Eq. (16) reads:

$$\begin{aligned}\frac{\mathrm{d}S_{\mathrm{tot}}}{\mathrm{d}t} &= \int_{\Omega}\left[\left(\frac{1}{{r^{\mathrm{b}}}^2}\frac{\partial {r^{\mathrm{b}}}^2 u_r}{\partial r^{\mathrm{b}}} - \frac{\partial u_r}{\partial r} + U_{\mathrm{d}}\frac{1}{{r^{\mathrm{b}}}^2}\frac{\partial {r^{\mathrm{b}}}^2}{\partial r^{\mathrm{b}}}\right)\overline{\Sigma}\right]\delta V \\ &\quad + \int_{\Omega}[S_{\mathrm{sgs}} + C_{\mathrm{sgs}}]\delta V \\ &= \frac{2}{r^{\mathrm{b}}}\int_{\Omega}\left[(u_r + U_{\mathrm{d}})\overline{\Sigma}\right]\delta V + \int_{\Omega}[S_{\mathrm{sgs}} + C_{\mathrm{sgs}}]\delta V \end{aligned} \tag{32}$$

In the first right-hand side term, $\int_\Omega (u_r + U_d)\overline{\Sigma}\delta V$ represents the burned gases volume growth rate due to the turbulent flame propagation. For a flame at constant pressure, this contribution is equal to: $(1+\tau)U_t S_{res} = (1+\tau)U_l \Xi S_{res} = (1+\tau)U_l S_{tot}$, where U_t is the turbulent flame speed. Eq. (32) then becomes:

$$\frac{1}{S_{tot}}\frac{dS_{tot}}{dt} = \frac{2}{r^b}(1+\tau)U_l + \frac{\int_\Omega [S_{sgs} + C_{sgs}]\delta V}{\int_\Omega \overline{\Sigma}\delta V} \tag{33}$$

In reality, the combustion does not take place at constant pressure, the combustion chamber being closed and gas compressibility effects exist. The speed of an iso-surface of flame surface density is then not $(1+\tau)U_l$ (Eq. (33)). In order to take into account these compressibility effects, a function Ψ is added to the first term on the right-hand side of this equation:

$$\frac{1}{S_{tot}}\frac{dS_{tot}}{dt} = \frac{2}{r^b}(1+\tau)U_l + \Psi + \frac{\int_\Omega [S_{sgs} + C_{sgs}]\delta V}{\int_\Omega \overline{\Sigma}\delta V} \tag{34}$$

It is difficult to propose a generic formulation for Ψ. Assuming this term is negligible compared to the strain rate by the eddies of the flow for very turbulent regimes, an expression for Ψ can be found that simply ensures the proper behavior of Eq. (34) for a laminar flow. Indeed, in the case of a laminar spherical flame, this equation writes:

$$\frac{1}{S_{tot}}\frac{dS_{tot}}{dt} = \frac{1}{S_{lam}}\frac{dS_{lam}}{dt} = \frac{2}{r^b}(1+\tau)U_l + \Psi \tag{35}$$

Moreover, the growth rate of the spherical flame can be expressed from the exact formulation of Eq. (13):

$$\frac{1}{S_{res}}\frac{dS_{res}}{dt} = \frac{1}{S_{lam}}\frac{dS_{lam}}{dt} = \frac{2}{r^b}(1+\tau)U_l - \frac{2}{3\gamma P}\frac{dP}{dt} \tag{36}$$

An expression accounting for the compressibility effects of Eq. (34) is obtained from the identification of Eqs. (35) and (36):

$$\Psi = -\frac{2}{3\gamma P}\frac{dP}{dt} \tag{37}$$

and the expression proposed by Duclos et al. [30] for the applications of the CFM model to engines is recovered.

Appendix B

The efficiency function of Charlette et al. [20] computes the strain induced by a turbulent flow on a premixed flame. This function Γ was built from DNS of elementary flame–vortex interactions at single length $r(k)$ and velocity $v'(k)$ scales: following a spectral analysis, DNS results were gathered into a single expression that accounts for all turbulent scales. Γ finally depends only on the laminar flame and largest turbulent scales properties, which correspond in the present work to U_l, δ_l, u' and l_t:

$$\left[\Gamma\left(\frac{l_t}{\delta_l}, \frac{u'}{U_l}, Re_t\right)\right]^2 = \frac{18}{55}C_k\pi^{4/3}\int_1^{+\infty} C_{CMV}\left(\frac{r(k)}{\delta_l}, \frac{v'(k)}{U_l}\right)^2 \kappa^{\frac{1}{3}} f(\kappa, Re_t)d\kappa \tag{38}$$

where $\kappa = kl_t/\pi$ is a dimensionless wave number, $Re_t = 4u'l_t/\delta_l U_l$ is the turbulent Reynolds number, $C_k = 1.5$ is a model constant and f and C_{CMV} are functions fitted on DNS results [20].

Appendix C

Using a combustion model based on the flame surface density transport equation, the Kolmogorov–Petrovski–Piskunov (KPP) theorem [31] may be used to derive a theoretical expression for the equilibrium turbulent flame speed U_t^{eq}. This derivation is based on the assumption of a steady turbulence and a planar mean flame propagation, allowing to express U_t^{eq} as a function of the fresh gases conditions and turbulence characteristics. For the equation considered here (Eq. (4)), one can show analytically that [28]:

$$U_t^{eq} = U_l + 2u'\sqrt{\frac{C\Gamma}{1 - \beta_c c^*/(1+\tau)}} \tag{39}$$

Introducing the steady state equilibrium factor as: $\Xi^{eq} = U_t^{eq}/U_l$ then leads to Eq. (20).

References

[1] G. Le Solliec, F. Le Berr, G. Colin, Y. Chamaillard, Oil Gas Sci. Technol. 62 (4) (2007) 555–572.
[2] F. Le Berr, G. Alix, S. Richard, F. Lafossas, et al., Powertrain simulation tools and application to the development of a SI engine concept car, SAE Technical Paper 2008-01-0356, 2008.
[3] F. Bozza, A. Gimelli, E. Torella, in: Proceedings of International Workshop on Diagnostics in Automotive Engines and Vehicles.
[4] S. Richard, G. Font, F. Le Berr, O. Grasset, et al., On the use of system simulation to explore the potential of innovative combustion systems: methodology and application to highly downsized SI engines running with ethanol–gasoline blends, SAE Technical Paper 2011-01-0408, 2011.
[5] G. D'Errico, A. Onorati, SAE Transact. 113 (4) (2004) 1–10.
[6] I. Wiebe, Halbempirische Formel fur die Verbrennungs-Geschwindigkeit, Verlag der Akademie der Wissenschaften der UdSSR, Moscow, 1956.
[7] J. Heywood, J. Higgins, P. Watts, R. Tabaczynski, Development and use of a cycle simulation to predict SI engine efficiency and NOx emissions, SAE Technical Paper 790291, 1979.
[8] P. Emery, F. Maroteaux, M. Sorine, J. Fluids Eng. 125 (2003) 520–532.
[9] G. Mauviot, A. Albrecht, T. Poinsot, A new 0D approach for diesel combustion modeling coupling probability density function with complex chemistry, SAE Technical Paper 2006-01-3332, 2006.
[10] S. Richard, S. Bougrine, G. Font, F.-A. Lafossas, F. Le Berr, Oil Gas Sci. Technol. 64 (2009) 223–242.
[11] O. Colin, A. Benkenida, Oil Gas Sci. Technol. 59 (2004) 593–609.
[12] S. Richard, O. Colin, O. Vermorel, A. Benkenida, C. Angelberger, D. Veynante, Proc. Combust. Inst. 31 (2007) 3059–3066.
[13] S. Bougrine, S. Richard, D. Veynante, Proc. Combust. Inst. 33 (2010), in press.
[14] S. Bougrine, S. Richard, D. Veynante, Modelling and simulation of the combustion of ethanol blended fuels in a SI engine using a 0D coherent flame model, SAE Technical Paper 2009-24-0016, 2009.
[15] B. Renou, A. Boukhalfa, Combust. Sci. Technol. 162 (2001) 347–371.
[16] S. Bougrine, S. Richard, J.-B. Michel, D. Veynante, Appl. Energy 113 (2014) 1195–1215, eRbib.
[17] S. Bougrine, S. Richard, A. Nicolle, D. Veynante, Int. J. Hydrog. Energy 36 (2011) 12035–12047, eRbib.
[18] D. Veynante, T. Poinsot, Reynolds averaged and large eddy simulation modeling for turbulent combustion, in: J.F.O. Metais (Ed.), New Tools in Turbulence Modelling, Springer, 1997, pp. 105–135, Lecture 5, Les editions de Physique, cONF.
[19] H. Weller, G. Tabor, A. Gosman, C. Fureby, Proc. Combust. Inst. 27 (1998) 899–907.
[20] F. Charlette, C. Meneveau, D. Veynante, Combust. Flame 131 (1–2) (2002) 159–180.
[21] R. Blint, Combust. Sci. Technol. 49 (1986) 79–92.
[22] J. Duclos, D. Veynante, T. Poinsot, Combust. Flame 95 (1993) 101–117.
[23] O. Colin, F. Ducros, D. Veynante, T. Poinsot, Phys. Fluids 12 (7) (2000) 1843–1863.
[24] T. Mantel, Contribution à la modélisation de la combustion dans les moteurs à allumage commandé avec prise en compte de la phase d'allumage, PhD thesis, Université de Rouen, France, 1993.
[25] T. Echekki, T.J. Poinsot, T. Baritaud, M. Baum, in: 8th International Symposium on Transport Processes in Combustion, San Francisco, 1995.
[26] B. Renou, Contribution à l'étude de la propagation d'une flamme de pré-mélange instationnaire dans un écoulement turbulent, PhD thesis, Université de Rouen, 1999.
[27] G. Woschni, A universally applicable equation for the instantaneous heat transfer coefficient in the internal combustion engine, SAE Technical Paper 670931, 1967.
[28] O. Vermorel, S. Richard, O. Colin, C. Angelberger, A. Benkenida, D. Veynante, Combust. Flame 156 (8) (2009) 1525–1541.
[29] G. Lacaze, B. Cuenot, T. Poinsot, M. Oschwald, Combust. Flame 156 (2009) 1166–1180.
[30] J. Duclos, G. Bruneaux, T. Baritaud, 3D modelling of combustion and pollutants in a 4-valve SI engine; effect of fuel and residuals distribution and spark location, SAE Technical Paper 961964, 1996.
[31] A. Kolmogorov, I. Petrovski, N. Piskunov, Bjul. Mosk. Gos. Univ. 1 (7) (1937) 1–72.